Inorganic Chemistry
Cite This: Inorg. Chem. XXXX, XXX, XXX−XXX
Article
pubs.acs.org/IC

A Lanthanide Luminescent Cation Exchange Material Derived from a Flexible Tricarboxylic Acid 2,6-Bis(1,2,3-triazol-4-yl)pyridine (btp) Tecton

Eoin P. McCarney,[†] Chris S. Hawes,[†] Jonathan A. Kitchen,[‡,∥] Kevin Byrne,[§] Wolfgang Schmitt,[§] and Thorfinnur Gunnlaugsson*[,†]

[†]School of Chemistry and Trinity Biomedical Sciences Institute (TBSI), Trinity College Dublin, The University of Dublin, Dublin 2, Ireland D02 R590

[‡]Chemistry, University of Southampton, Southampton SO17 1BJ, U.K.

[§]School of Chemistry and Centre for Research on Adaptive Nanostructures and Nanodevices (CRANN), Trinity College Dublin, The University of Dublin, Dublin 2, Ireland D02 XR15

Supporting Information

ABSTRACT: The synthesis of the three-dimensional metal−organic framework material, $[Zn_7L_6]\cdot(H_2NMe_2)_4\cdot(H_2O)_{45}$ (**1**), derived from a flexible tricarboxylic acid 2,6-bis(1,2,3-triazol-4-yl)pyridine (**btp**) ligand, is presented. The **btp** ligand, H_3L, adopts a three-dimensional hydrogen bonding network in the crystalline state through a combination of carboxylic acid dimer and *syn*−*anti*-**btp**/carboxylic acid hydrogen bonding synthons. The Zn(II) species **1** exhibits a three-dimensional framework structure with the rare **crs** topology and contains linear and undulated solvent channels extending in three dimensions. The guest exchange and gas adsorption properties of **1** were investigated; herein we demonstrate the exchange of dimethylammonium cations from the as-synthesized material with cationic guest molecules in the form of dyes and luminescent Ln(III) ions. Sensitization of Eu(III) and Tb(III) inside the porous network of **1** was achieved upon cation exchange, with a view toward developing functional luminescent materials.

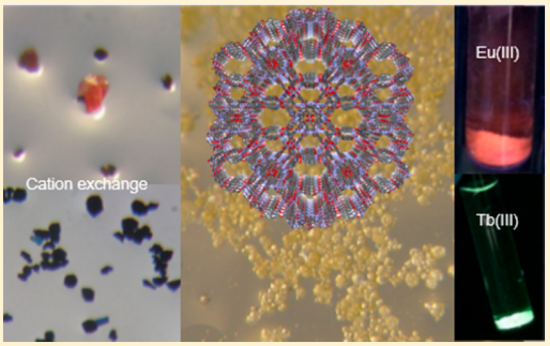

INTRODUCTION

Metal−organic frameworks (MOFs) represent a swiftly advancing research area in chemical and material sciences, continuously intriguing scientists not only by the extensive range of affordable network topologies[1] but also by their applicable properties,[2] such as catalysis,[3] sensing,[4] guest encapsulation,[5] and gas adsorption and separation.[2,6] Moving beyond the typical rigid-ligand designs of early MOFs, reports of MOFs derived from divergent ligands possessing at least one flexible sp^3 linker group are now becoming commonplace.[6d,7] The low-energy bond rotations in these systems create a range of bridging geometries, facilitating the development of more dynamic or "breathable" systems.[8] However, this class of semirigid ligand can also generate rigid frameworks through increased connectivity in more than two directions.[9] Drawbacks associated with such flexible-ligand MOFs[7a] include an impeded control over the rational structural predictability of extended network architectures.[10] However, conformational adaptability of the ligand precursor can be advantageous when combined with a labile metal ion's energetically preferred coordination geometry, thus facilitating the generation of structurally diverse MOFs whose architectures would not be attainable from more rigid building blocks.

The terdentate heteroaromatic 2,6-bis(1,2,3-triazol-4-yl)-pyridine (**btp**) motif has been featured frequently in the literature in recent times and has been incorporated into amorphous polymers and macromolecules through metal-templated synthesis,[11] as well as in the formation of metallo-supramolecular gels.[11e,12] Reports of MOFs featuring the 1,2,3-triazole motif[13] and, to a greater extent, the 1,2,4-triazole motif[3c,5,6c,e,f,14] have become relatively ubiquitous in the literature; however, there are no reports of **btp** derived MOFs. The **btp** motif has been shown to form stable coordination complexes with both transition and trivalent lanthanide (Ln(III)) ions.[15] Its variability is useful when greater versatility is desirable compared to the analogous 2,2′-6′,2″-terpyridine,[11e,16] with a broad range of derivatives available through "click" chemistry.[17] Thus, convenient development of neutral nitrogen containing **btp** heterocycle linkers possessing rich coordination chemistry capable of generating functional MOFs is readily achieved through the facile incorporation of divergent metal binding ability in the form of multiple carboxylate functionality.[18] With this in mind, we set out to demonstrate the synthesis of a three-dimensional anionic MOF

Received: January 9, 2018

DOI: 10.1021/acs.inorgchem.8b00080
Inorg. Chem. XXXX, XXX, XXX−XXX

using the flexible **btp** ligand, H_3L. The tricarboxylic acid H_3L contains four distinct functional groups capable of metal coordination: the **btp** terdentate chelating motif and the three carboxylate groups (upon deprotonation). Herein we demonstrate that the coordination of the terdentate motif with metal ions results in conformational switching in **btp**; in the presence of a cation the *syn*−*syn* conformation[12a,c,d,15a,17b] is observed (Scheme 1).

Scheme 1. Conformational Changes of the btp Motif (left) and of the Aryl Arms around the Methylene Linker (right)

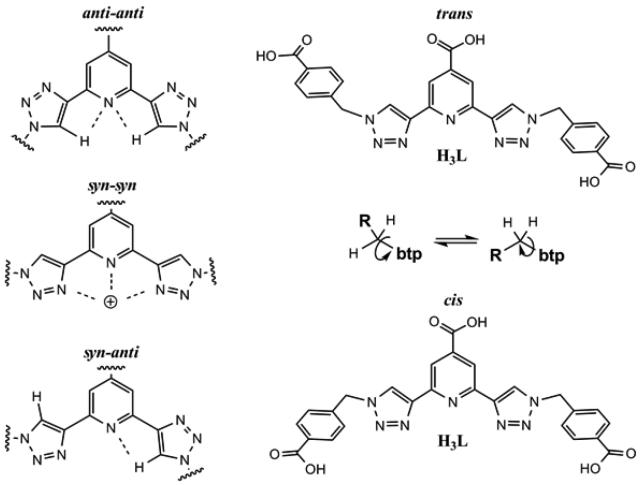

However, the unbound **btp** moiety displays triazoles *anti*−*anti* (or "kinked") with respect to the pyridyl nitrogen atom[11e,12d,17b,19] due to the nitrogen lone pair repulsion and an intramolecular hydrogen bonding interaction between the triazole hydrogen atoms and the pyridyl nitrogen atom.[11e] There is also a third possibility, the *syn*−*anti* conformation. The multiple coordinating directionality together with the conformational freedom of semirigid ligands like H_3L makes them very appealing for the design of new architecturally diverse MOFs which also possess desirable functional properties.

The unique chemical and physical properties of MOFs have ensured that they continue to be the focus of much scientific attention.[10] These properties, including luminescence,[8b,20] chemical separation,[21] sensing,[4a,b,21] and ion exchange,[14a,22] among others,[8a] arise from their ability to adsorb and recognize specific guests through various host−guest interactions within rationally designed, monodisperse pores. The uptake of specific guests by MOFs in the development of luminescent materials has potential for application in fluorescent sensing and in the development of next generation solid state lighting devices, display technologies, and other lighting applications.[23] Charge balancing cations such as Ln(III) ions, namely Eu(III) and Tb(III), are ideal components in an anionic framework luminescent MOF where the host material is capable of the required sensitization; these can be incorporated through a cation exchange process from the as-synthesized material, of which several have been reported to date.[24] The Eu(III) and Tb(III) radiative excited states are not heavily perturbed by ligand field effects, giving rise to line-like emission and pure colors of red and green, respectively. With this in mind, herein we report the synthesis, cation exchange, and Ln(III) centered phosphorescence studies of an anionic MOF from the structurally versatile polytopic tricarboxylic acid **btp** ligand H_3L.

RESULTS AND DISCUSSION

The heteroaromatic **btp** ligand H_3L, the synthesis of which was previously reported as part of recent gelation studies with Eu(III),[12c] was crystallized by evaporation from CH_3OH. The diffraction data were collected, and the structure model was refined in the monoclinic $P2_1/c$ space group with one molecule in the asymmetric unit (Figure 1). Crystallographic refinement details can be found in Table 1. Powder X-ray diffraction (PXRD) analysis confirmed the phase purity (Figure S28 in Supporting Information).

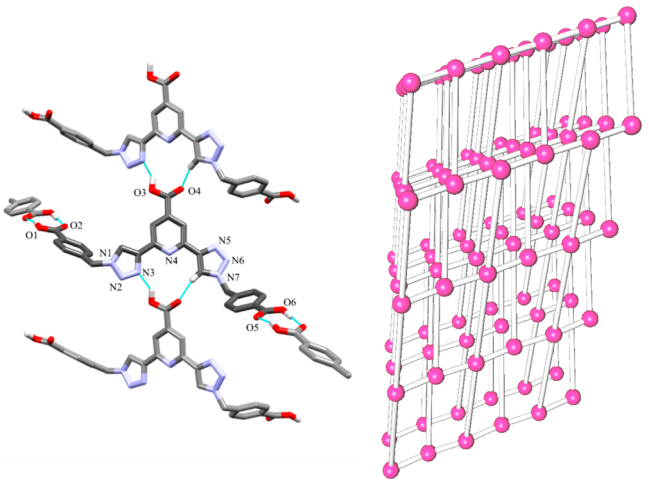

Figure 1. (left) X-ray crystal structure of tricarboxylic acid **btp** ligand H_3L displaying a three-dimensional hydrogen bonded network. Hydrogen atoms not involved in hydrogen bonding interactions omitted for clarity. (right) Topology diagram for the **cds** network formed by H_3L with each of the pink spheres representing the four connecting nodes defined by H_3L molecules.[25]

The pyridyl and two triazolyl units are essentially co-planar. The planar conformation of **btp** facilitates the $\pi-\pi$ stacking interactions among molecules along the *b* axis; the perpendicular distance between the parallel mean planes of **btp** cores is 3.290(3) Å. The benzoic acid arms adopt a *trans*-like conformation relative to the central **btp** core, facilitating packing along the *a* and *b* axes through two pairs of $R_2^2(8)$ cyclic carboxylic acid dimers per molecule[26] (the distances and angles for the two donor−acceptor pairs: d(D···A) is 2.574(4) Å, ∠(O−H···O) is 173.7(2)°; d(D···A) is 2.665(4) Å, ∠(O−H···O) is 162.32(15)°). The **btp** *syn*−*anti* orientation facilitates extension of the network in the remaining *c* axis direction through an $R_2^2(12)$ motif.[26] The proximal N3 atom of one triazole ring faces in toward the pyridyl nitrogen atom as the former acts as a hydrogen bond acceptor for the carboxylic acid O3 hydrogen bond donor (d(D···A) is 2.668(4) Å, ∠(O−H···N) is 143.78(17)°). Simultaneously, the proximal N5 of the other triazole unit is rotated away from the pyridyl nitrogen atom, resulting in a hydrogen bonding interaction between the triazolyl C−H hydrogen bond donor and the 4-pyridyl carboxylic acid O4 acceptor (d(D···A) is 3.075(4) Å, ∠(C−H···O) is 163.4(2)°). This is, to the best of our knowledge, the first time this **btp** conformation has been observed in the crystalline phase, contrasting with the more common *syn*−*syn* orientation[11e,12c,d,15,17b,19g,27] adopted when chelation of a metal ion occurs and the *anti*−*anti* conformation,[11e,12d,17b,19] which is observed for the unbound ligand.

DOI: 10.1021/acs.inorgchem.8b00080
Inorg. Chem. XXXX, XXX, XXX−XXX

Table 1. Crystallographic Refinement Details for H_3L and Compounds 1 and 2

	H_3L	1	2
empirical formula	$C_{26}H_{19}N_7O_6$	$C_{156}H_{96}N_{42}O_{36}Zn_7$	$C_{26}H_{17}N_7O_6Zn$
formula weight	525.48	3592.33	588.83
temperature (K)	100(2)	100(2)	100(2)
crystal system	monoclinic	cubic	monoclinic
space group	$P2_1/c$	$Fd\bar{3}$	$C2/c$
a (Å)	20.486(4)	51.459(2)	21.9888(15)
b (Å)	7.1760(14)	51.459(2)	17.8548(13)
c (Å)	17.144(3)	51.459(2)	10.4152(7)
α (deg)	90	90	90
β (deg)	111.00(3)	90	115.420(5)
γ (deg)	90	90	90
volume (Å^3)	2352.9(9)	136266(13)	3693.2(5)
Z	4	16	4
ρ_{calc} (g cm^{-3})	1.483	0.700	1.059
μ (mm^{-1})	0.109	0.896	1.264
$F(000)$	1088.0	29184.0	1200.0
radiation source	Mo Kα	Cu Kα	Cu Kα
2θ range (deg)	4.76 to 49.99	4.86 to 137.36	6.66 to 136.59
reflns collected	22769	96561	5909
independent reflns	4142 [R_{int} = 0.0949, R_{sigma} = 0.0751]	10477 [R_{int} = 0.1232, R_{sigma} = 0.0561]	3381 [R_{int} = 0.0669, R_{sigma} = 0.0732]
reflns obs [$I \geq 2\sigma(I)$]	2915	5095	2504
data/restraints/parameters	4142/0/352	10477/0/363	3381/0/187
GOOF on F^2	1.130	0.988	0.962
R indices [$I \geq 2\sigma(I)$]	R_1 = 0.0741, wR_2 = 0.1393	R_1 = 0.1083, wR_2 = 0.2888	R_1 = 0.0524, wR_2 = 0.1293
R indices [all data]	R_1 = 0.1136, wR_2 = 0.1548	R_1 = 0.1430, wR_2 = 0.3293	R_1 = 0.0716, wR_2 = 0.1400
largest diff peak/hole (e Å^{-3})	0.25/−0.30	0.57/−0.74	0.48/−0.45
CCDC number	1582309	1582310	1582311

Each **btp** molecule is connected to four other neighboring molecules as a result of the hydrogen bonding, giving rise to an overall 4-fold interpenetrated three-dimensional extended structure (Figure S2). The nets are described by the **cds** topology, where each H_3L molecule is defined as a 4-connecting node (Figure 1).[25] In the idealized **cds** topology, square planar nodes connect to orthogonally oriented square planar nodes. This is manifested in the crystal structure of H_3L by an ABAB packing fashion along the c axis with the mean planes defined by the atoms comprising the **btp** moieties in alternating A and B layers twisted relative to each other by an angle of 45.97(15)° (Figure S1), as opposed to 90° in the idealized **cds** topology.

The crystal structure also shows that despite the symmetric nature of the ligand there was no disorder detected over the two triazole ring junctions, each possessing 100% occupancy in their respective orientations throughout the system. The study of the solid state structure of H_3L provides insights into the molecular geometry of such compounds known to form gels through similar hydrogen bonding interactions (the synthesis, morphological, and rheological studies of the hydrogel of H_3L have been previously reported as stated above).[12c] This is an area in which there is a large gap between design efforts and actual knowledge of the supramolecular structure of the gels (i.e., the molecular arrangement of gelator molecules within the gel fibers, the junction zones, etc.).[28]

Synthesis and Structure of Poly-$[Zn_7L_6]\cdot(H_2NMe_2)_4\cdot(H_2O)_{45}$ (1). Faint yellow hexagonal crystals of **1** were obtained upon reaction of H_3L and zinc(II) nitrate hexahydrate in a mixture of 95:5 DMF/H_2O in a sealed vial heated to 100 °C. The reaction was complete after 40 h. A second crystalline phase (**2**) was present in the initial reaction mixture possessing Zn:**HL** (1:1) stoichiometry. Although **2** could be characterized crystallographically (Supporting Information), we were unable to reproducibly generate the phase selectively. Via optimization of the synthesis, such that the zinc(II) nitrate hexahydrate was present in slight excess (1.2 equiv), the coordination polymer with formula poly-$[Zn_7L_6]\cdot(H_2NMe_2)_4\cdot(H_2O)_{45}$ was exclusively produced in high yield as confirmed by powder XRD analysis (Figure S29). The asymmetric unit contains one molecule of **L** and two unique zinc sites; one of these sites is present at full crystallographic occupancy, while the other occupies a special position, with a total of 1 $^1/_6$ Zn atoms per molecule of **L** (i.e., Z' = 0.16667).

There are four dimethylammonium cations, which could not be located crystallographically, for every Zn_7L_6 repeat unit for charge balance. The nature of the cations was instead ascertained using IR and NMR spectroscopy; in the IR spectrum of **1** after soaking with CH_3CN, a broad absorbance at 2977 cm^{-1}, typical for cationic ammonium N−H stretches, indicated the presence of dimethylammonium.[29] The digestion of the crystals of **1** in deuterated TFA allowed the characteristic dimethylammonium proton resonances to be seen in the ^{1}H NMR spectra at 2.89 ppm, integrating appropriately in a 4:4 ratio accounting for an L_6/(dimethylammonium)$_4$ stoichiometric ratio (Figures S12 and S13). The dimethylammonium cations most likely originate from *in situ* hydrolysis of the DMF solvent.[30] The total contents of the channels of an air-dried sample of **1** were determined by the combination of thermogravimetric and elemental analysis, suggesting a void content, in addition to the four dimethylammonium charge balancing counterions, of 45 H_2O molecules per Zn_7L_6 formula unit. This was correlated to the electron count provided by SQUEEZE,[31] which is in good agreement (see SI).

DOI: 10.1021/acs.inorgchem.8b00080
Inorg. Chem. XXXX, XXX, XXX−XXX

The structural model for **1** was refined in the cubic $Fd\bar{3}$ space group manifesting as a three-dimensional coordination polymer. The extended system is comprised of two distinct coordination environments (Figure 2); Zn1 displays a pseudo-

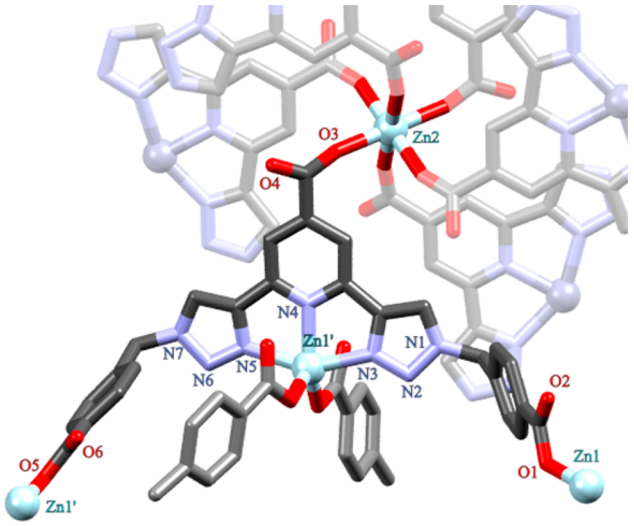

Figure 2. Fragment view of the crystal structure of **1** showing the connectivity of the two unique Zn(II) coordination environments.

trigonal bipyramidal coordination environment as a result of the **btp** *syn*–*syn* chelation and the binding of two monodentate carboxylate oxygen atoms on the benzyl arms of two adjacent ligands.

The geometry of Zn1 shows some deviation from that of an idealized trigonal bipyramid with a value of τ_5 = 0.72.[32] The basal plane of the coordination polyhedron consists of the pyridyl N4 atom and the pair of monodentate carboxylate oxygen atoms, O1 and O5, whereas the apical sites are occupied by the two proximal triazolyl nitrogen atoms, N3 and N5. The bite angles ∠(N3–Zn1–N4) and ∠(N4–Zn1–N5) are 76.6(2)° and 74.4(2)°, respectively. The N4–Zn1 bond length is 2.081(6) Å, and the N–Zn distances are 2.158(6) and 2.206(6) Å for triazole atoms N3 and N5, respectively. The O1–Zn1 and O5–Zn1 bond lengths are 1.924(4) and 1.937(4) Å, respectively. The second unique Zn(II) coordination environment has an octahedral character and is coordinated by six monodentate carboxylate groups. This coordination environment is particularly unusual; crystallographically characterized examples of fully monodentate [Zn(RCOO)$_6$] centers have until now been reported in only homo- or heterometallic clusters featuring μ_2-κO;κO′ bridging to additional metal ions. This bridging is usually brought about by the formal 4– charge of the central coordination sphere. However, in the present case, the noncoordinating oxygen atoms are involved in C–H···O hydrogen bonding interactions with the nearby triazole C–H groups (d(C···O) 3.003(9) Å, ∠(C–H···O) is 149.1(4)°), negating their ability to coordinate to an additional cation. The two C–O bonds are the same length within error, consistent with a fully ionic carboxylate rather than the more localized bonding mode observed in Zn1. This highly Lewis basic site is the most likely candidate for hydrogen bonding interactions with the intractably disordered dimethylammonium cations. A similar hydrogen bonding interaction also occurs involving the noncoordinating oxygen atoms from the Zn1 coordination sphere and is common for **btp** and other 1,2,3-triazole containing species. The octahedral Zn2 node links six **btp** ligands, each coordinating through the 4-pyridyl carboxylate position. All six metal–ligand bonds are equivalent (the O1–Zn2 distance is 2.087(6) Å), as the Zn2 atom resides coincident with crystallographic improper rotation axes.

The intricate connectivity of **btp** and zinc ions within complex **1** makes direct comparison of the topology to a known three-dimensional net challenging. Avoiding the nontrivial trinodal 3,4,6-connected network description arrived at by assigning nodes to each unique metal and ligand, we arrived at the most sensible topological description by assigning a six-connected node to the central octahedral zinc ion Zn2 which further encompasses all six of the coordinated ligand molecules and their **btp**-chelated Zn1 ions (Figure 3). With this

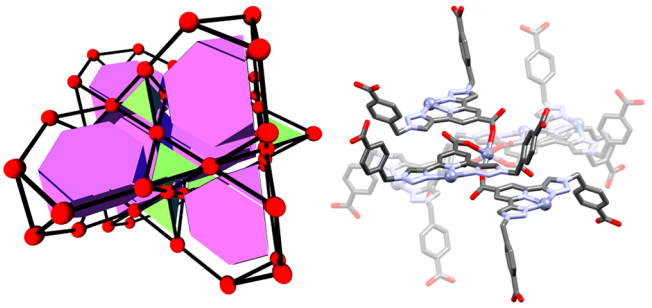

Figure 3. (left) Graphical representation of the idealized **crs** topology.[25] (right) The fragment view of the six connecting nodes represented by the red spheres in the **crs** topological diagram.

description, the network "links" are simply the Zn–carboxylate bonds involving Zn1, and each of these nodes as defined above links to only six others. Any two adjacent nodes are linked to each other by 4 Zn–carboxylate links occurring through the pair of symmetry related Zn1–O1 and Zn1–O5 bonds (Figure S3). The resulting network topology, although somewhat esoteric, is described by the **crs** (cristobalite) net,[25] equivalent to the augmented **dia-e** net. The six-connecting nodes result in a net of edge-sharing truncated tetrahedra ([3^4·6^4], purple) and smaller tetrahedra ([3^4], green).[33] No interpenetration was evident in the structure of **1**.

The crystal packing is dominated by rhomboidal cages connected face-to-face to four equivalent cages by the octahedral Zn2 centers (Figure S4). The remaining two faces, not occupied by Zn2 octahedral sites, are directed into the large solvent channels, which exist in all three dimensions (Figure 4).

A mixture of straight channels and undulated channels are interconnected; the three-dimensional network of pores, in total, account for approximately 45% of the total unit cell volume. It should be noted that, taking into account the dimethylammonium cations (64 of which per unit cell, which account for only ca. 2.5% of the total unit cell volume), the volume of these channels still allows for considerable solvent-accessible volume. These channels are irregularly hexagonal in nature and alternate between two distinct sizes, i.e., approximately 21 and 14 Å at their maximum edge-to-edge interatomic distances, respectively (Figure S5). The aromatic rings of the ligand benzoate arms dominate the makeup of the edges of the two differing hexagonal channels with the Zn1 centers at each of the six corners. Following the elucidation of the channel system in the structure of **1**, we turned our attention to guest exchange studies.

DOI: 10.1021/acs.inorgchem.8b00080
Inorg. Chem. XXXX, XXX, XXX–XXX

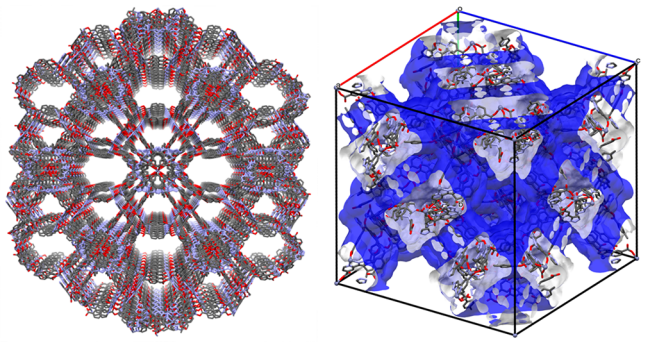

Figure 4. (left) Perspective view of the solvent channels in the crystal structure of **1**, with the hydrogen atoms omitted for clarity. (right) Perspective view of the solvent-accessible surface (blue) highlighting the channels that exist in a single unit cell.

Thermal and Gas Adsorption Studies. Thermogravimetric analysis (TGA) of freshly isolated **1** revealed a multistep desolvation profile upon heating in a nitrogen atmosphere (Figure S6). The freshly prepared, predominantly DMF-filled compound experienced a loss in mass between approximately 60 and 120 °C, which then flattened at 160 °C between 65% and 61% residual mass before another sharp decrease in mass occurred at 350 °C due to decomposition. The total loss in mass was approximately 39% (wt) in the 40 → 350 °C temperature range. After **1** was soaked in MeCN, a rapid loss in mass was observed beginning at room temperature and reaching a plateau at approximately 73% residual mass below 100 °C (Figure S7). From these data it can be concluded that the lattice solvent molecules in **1** are readily exchanged for the more volatile MeCN upon soaking.

The effect of exposing a sample of **1** to the atmosphere was also investigated using thermogravimetric analysis. The thermal profiles of samples of **1** which had been air-dried over the course of four months were strikingly similar (Figure S7) and in contrast to that of a freshly prepared sample comprised predominantly of DMF, as observed by ^{1}H NMR of the digested fresh sample (Figure S13). There was a more substantial loss in mass for the freshly prepared sample but a lesser loss in mass for samples which were air-dried, indicative of the channel solvent being exchanged with water in the atmosphere. This observation explains why the thermal profiles of **1**, regardless of initial solvent occupying the channels (DMF or MeCN), behave similarly after exposure to the atmosphere for an extended period. An intermediate stage of solvent exchange with atmospheric water shows a lesser extent of volatile mass loss (Figure S7) due to the shorter four week period of time it was in contact with the atmosphere. This observation that DMF solvent molecules had been exchanged with water molecules was corroborated after elemental analysis on an air-dried sample, which indicated the presence of water within the channels and could not be suitably fitted due to DMF within the channels.

On the basis of the substantial capacity of **1** for neutral guest molecules, gas adsorption experiments were also undertaken. Following CH_3CN exchange, the sample was activated at 100 °C under dynamic vacuum overnight. Surprisingly, the CO_2 (273 K), H_2 (77K), and N_2 (77K) adsorption isotherms showed much lower than expected uptake for the thermally activated material (Figures S8−10), with a maximum loading of ~3.75 wt % CO_2 at 1 atm and 278 K and lower loadings for N_2 and H_2. These data suggest that the large and interconnected channels in the as-synthesized material are contracted or collapsed following evacuation. X-ray powder diffraction analysis of the CH_3CN exchanged material showed a loss of crystallinity after drying (see Figure S30). This outcome is disappointing for a three-dimensional framework material; nonetheless, such instability can be rationalized as a consequence of the flexibility of the **btp** ligand supporting the bulk material and may also be related to the expected lability of the pivotal Zn2 node.

Cation Exchange Experiment. Due to the apparent reduction in free volume of **1** upon evacuation, an alternative investigation into the guest uptake properties was undertaken, taking advantage of the anionic framework of **1**. It was found that soaking **1** in concentrated solutions of cationic dyes, such as ethidium bromide and methylene blue, for 3 days resulted in uptake of the dyes, evident from a color change observed in the individual crystals (Figure 5).

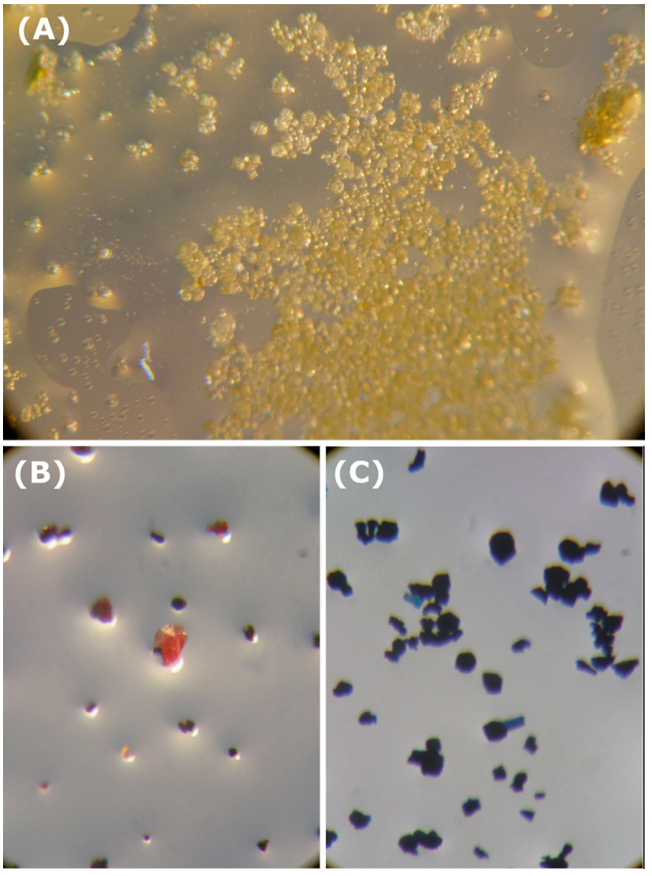

Figure 5. Optical microscope photographs of crystals of **1** (A) before cation exchange and after cation exchange with (B) ethidium bromide and (C) methylene blue.

To confirm that this color change was not simply surface adsorption of the dye, the crystals were soaked with CH_3CN solution for several days until the supernatant ran colorless; after this time no further leeching of dye into the supernatant was observed. The characteristic red color and blue color of ethidium bromide and methylene blue, respectively, can clearly be seen in the thinner and more transparent crystals, whereas the thicker larger crystals appeared opaque. The CH_3CN solvent was then replaced with a concentrated stock solution of tetraethylammonium iodide (TEAI) in CH_3CN. Immediately

DOI: 10.1021/acs.inorgchem.8b00080
Inorg. Chem. XXXX, XXX, XXX−XXX

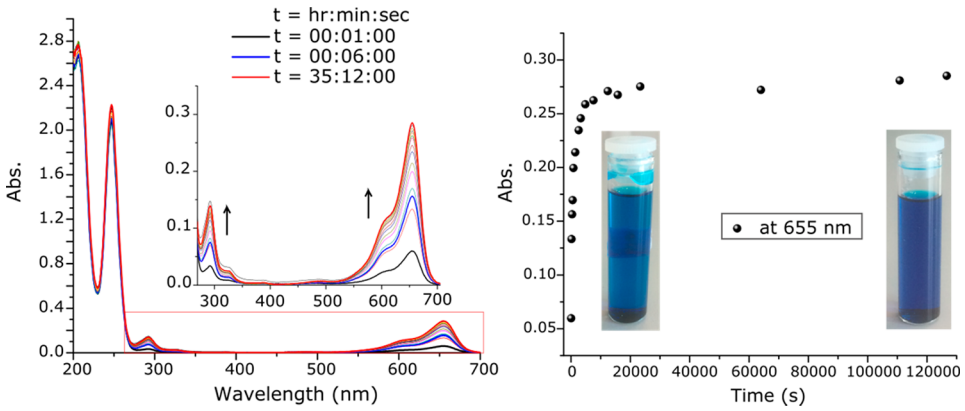

Figure 6. Changes in the UV−vis spectrum of the supernatant of **1** (6 mg) previously soaked in a concentrated solution of methylene blue in CH_3CN upon addition of triethylammonium iodide in CH_3CN (c = 16.4 mM, 4 mL) solution at 21 °C.

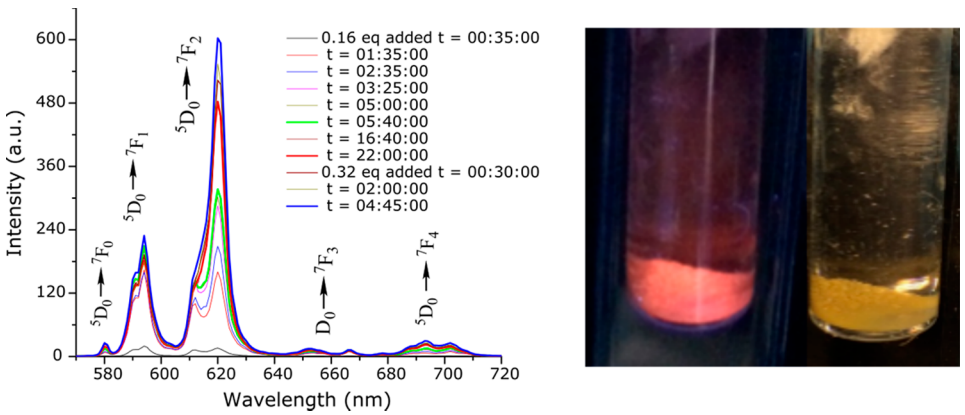

Figure 7. (left) Observed Eu(III) centered phosphorescence increasing with time after compound **1** (11 mg, 3.49 μmol) was treated with $Eu(CF_3SO_3)_3{\cdot}6H_2O$ in CH_3CN solution (0.58 mM, 1 mL, 0.16 equiv) and (right) crystals of **1** under 365 nm UV radiation and in daylight.

upon addition the supernatant took on the color of the escaping dye molecules as they were exchanged with the TEA cations. Specific aliquots of the supernatant solution were taken at defined time intervals, and the indicative absorbance was recorded. In each case, the dye-loaded samples showed a release of the respective dye molecule into the supernatant. The absorbance plot and release profile for methylene blue are shown in Figure 6.

Bands at 204 and 247 nm did not undergo any significant changes indicative of the excess TEAI in the solution mixture, while the absorbance of the bands at 293 and 655 nm increased as the methylene blue guest molecules were liberated from the solid **1**. The concentration increased substantially until between 90 and 120 min after the TEAI solution was added, and at this point no further increase was observed. The changes in the absorption spectrum could be quantified using the measured extinction coefficient of methylene blue in CH_3CN, measured in a 16.4 mM solution of TEAI in CH_3CN (UV−vis (MeCN) λ_{max}/nm (ε_{max}/dm^3 mol^{-1} cm^{-1}): 291 (37,000), 655 (77,000)). The amount of methylene blue dye released from the first TEAI soaking corresponds to 23% of the total cationic species required for charge balance within the framework. Further release of dye was observed when a fresh solution of TEAI (3 mL) was added to the same sample of **1** after removal of the original supernatant (Figure S17), and the release was at its maximum between 100 and 150 min after which no further substantial increase was observed. It was calculated from this that a further 8% of dye had been exchanged. A third replacement of the supernatant with a fresh solution of TEAI in CH_3CN gave rise to a further release of 4% of dye (Figure S18). In each case, the blue color of the crystals remained evident following soaking, indicating that complete removal of the dye guest was not forthcoming under these conditions. The same cation exchange was carried out with ethidium bromide solution in CH_3CN (Figure S19). Approximately 9% of the total cationic species, in the form of the ethidium cation, was released when TEAI solution was added. The samples were then digested in deuterated TFA; the ^{1}H resonance of 2.91 ppm indicative of the dimethylammonium cation was not observed in the dye-soaked, TEAI-exchanged samples (Figure S14). The small amount of methylene blue and ethidium bromide still present in the samples accounted for the release of blue and red colors, respectively, into solution upon digestion of the crystals in TFA-d_1. In particular, the residual methylene blue was evidenced by the diagnostic methyl resonance at 3.59 ppm (Figure S15) which integrated to 0.4 proton per **L**, equating to <10% of the total cationic species. This also contributes to the explanation of why the total amount of methylene blue released by exchange with TEAI solution was observed to be less than the total possible. However, the most contributory factor to the total release of methylene blue, accounting for only approximately ca. 35% of the amount expected, is most likely the less than complete exchange of the dimethylammonium cation. However, the remaining dimethylammonium was efficiently replaced by TEA during the second cation exchange step. Integration of the ^{1}H NMR resonance

DOI: 10.1021/acs.inorgchem.8b00080
Inorg. Chem. XXXX, XXX, XXX−XXX

indicative of a TEA cation at 3.29 and 1.38 ppm shows the exchange with methylene blue, and any original dimethylammonium was almost quantitative, i.e., 6:4 (**L**/TEA) ratio evidenced by peaks *e*,1, and 2 integrating in a 1:1.33:2 ratio (Figure S15).

The smaller volume of the TEA cation and higher concentration of the stock solution used relative to methylene blue most likely account for the more favorable uptake by **1**. For this same reason, methylene blue was less efficient compared to TEA in the replacement of the dimethylammonium cation initially but was more favorable than the substantially larger ethidium cation. Although complete exchange of the lattice cations in **1** with larger cations was not observed, the uptake of up to 35% of methylene blue, and complete exchange for tetraethylammonium, is an encouraging observation for the use of **1** as a cation exchange material and implies the retention of a considerable solvent-accessible volume.

Spectroscopic Monitoring of Ln(III) Exchange and Sensitization Studies. It is well-known that the **btp** terdentate motif is capable of sensitizing Ln(III) luminescent states[11e,15a,16,19c] with some reports achieving photoluminescence quantum yields of 70% in CH_3CN solution.[34] With this in mind, and encouraged by the ability of **1** to readily undergo cation exchange, we treated a sample of **1** which had been previously soaked in CH_3CN initially with $Eu(CF_3SO_3)_3{\cdot}6H_2O$ solution in CH_3CN, containing 0.16 equiv of Eu(III) with respect to **1**. Sensitization of Eu(III) by **1** occurred immediately, evidenced by the characteristic red phosphorescence emitted from the crystals of **1** under UV radiation at 365 nm, which was clearly visible to the naked eye as demonstrated in Figure 7. It should be noted that prior to exchange with Ln(III) ions, the as-synthesized **1** did not display any measurable luminescence whatsoever, despite using a range of UV excitation wavelengths. The phosphorescence changes were also monitored at specific time intervals (Figure 7).

Eu(III) centered phosphorescence intensity plateaued when **1** was treated with dilute $Eu(CF_3SO_3)_3{\cdot}6H_2O$ in CH_3CN (1 mL, 0.16 equiv, 0.32 equiv with respect to **1**). Upon addition of more concentrated solutions (1 mL, 3.5 equiv with respect to **1**) further increases in phosphorescence intensity were observed over time. It should be noted that the absolute phosphorescence intensities could not be quantitatively determined as a function of time due to the unpredictable scattering and packing effects of the solid materials. Nonetheless, we observed an unmistakable qualitative increase in overall phosphorescence intensity (further details of the Eu(III) sensitization experiment can be found in the Supporting Information). The lanthanide emission was shown to be rapidly quenched upon addition of TEAI in CH_3CN solution (6.39 mM, 1 mL) (Figure S27). This is a result of the rapid displacement of the cationic Eu(III) ions by the TEA cations.

The same experiment was carried out with Tb(III) by treating a sample of **1** which had been previously soaked in CH_3CN with a $Tb(CF_3SO_3)_3{\cdot}6H_2O$ solution in CH_3CN (0.16 equiv with respect to **1**). Immediately, sensitization of Tb(III) occurred, which was evidenced by the characteristic green phosphorescence emitted from the crystals of **1** under UV radiation at 365 nm, as shown in Figure 8.

As before, the Tb(III) emission changes were monitored at specific time intervals showing an increase in Tb(III) centered phosphorescence over time. To begin, a dilute solution of Tb(III) was added (1 mL, 0.16 equiv with respect to **1**), and as

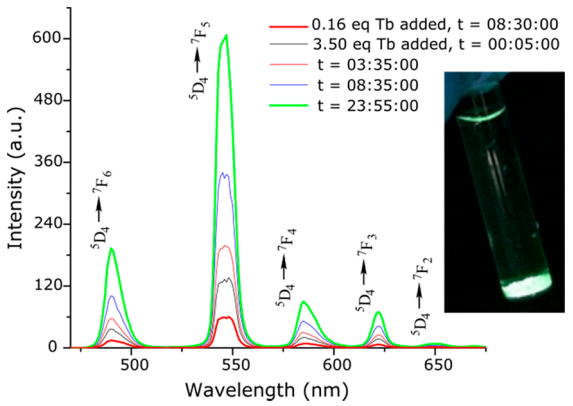

Figure 8. Tb(III) centered emission observed after treatment of **1** with a solution of $Tb(CF_3SO_3){\cdot}6H_2O$ in CH_3CN (3.5 equiv with respect to **1**) increasing with time. (Inset) Crystals of **1** under 365 nm UV radiation.

in the case of the Eu(III), upon addition of more concentrated solutions (3.5 equiv with respect to **1**) further increases in the phosphorescence intensity were observed over time (further details of the Tb(III) sensitization experiment can be found in the Supporting Information, including blending of the red and green colors emitting from **1**). It was also investigated if there was any leeching of ligand from the extended structure of **1** by taking UV−vis spectra of the supernatants of each sample. There was no indication of **btp** absorption bands observed (Figure S25 (left)). We also concluded that the metal centered phosphorescence was produced exclusively by the crystals after it was confirmed there was no phosphorescence observed from the supernatants when crystals of **1**-Eu and **1**-Tb were not in the beam path (Figure S25 (right)).

Radiative lifetime studies were also carried out, displaying bi-exponential radiative decay curves indicative of two Eu(III) environments and two Tb(III) environments in **1**-Eu and **1**-Tb, respectively. The observed radiative lifetimes had values on average of τ_1 = 0.48(01) ms and τ_2 = 1.91(10) ms for the Eu(III) species and on average of τ_1 = 0.92(01) ms and τ_2 = 4.45(14) ms for the Tb(III) species. A summary of the observed lifetimes is presented in Table S1 of the Supporting Information.

CONCLUSION

A three-dimensional anionic coordination polymer, **1**, with the formula $[Zn_7L_6]{\cdot}(H_2NMe_2)_4{\cdot}(H_2O)_{45}$ derived from a semi-flexible tricarboxylic acid **btp** ligand was synthesized in good yield with excellent bulk purity achieved. A second crystalline phase, **2**, which was present as a byproduct in initial attempts, was successfully removed through synthetic optimization. The extended structure of **1** was characterized using conventional methods: single crystal and powder X-ray diffraction analysis and gas adsorption studies together with thermogravimetric and elemental analysis. A crystal structure of the **btp** ligand, H_3L, was also obtained, displaying a three-dimensional hydrogen bonding network. While a reduction in void volume was observed following the complete evacuation of **1**, efficient guest exchange was observed in solution, using cationic dye molecules as probes. Uptake and sensitization of Eu(III) and Tb(III) within the framework of **1** was also achieved. These observations demonstrate the potential of materials exhibiting poor structural resilience to complete evacuation, such as **1**, as nonetheless useful cation exchange matrices for the develop-

DOI: 10.1021/acs.inorgchem.8b00080
Inorg. Chem. XXXX, XXX, XXX−XXX

ment of functional luminescent materials. Efforts are currently being made to appropriately tune the uptake of various luminescent guests by **1** in the pursuit of customizable white light emitting materials.

EXPERIMENTAL SECTION

Materials and Methods. All solvents and chemicals were purchased from commercial sources and used without further purification.

Melting points were determined using an Electrothermal IA9000 digital melting point apparatus and are uncorrected. Infrared spectra were recorded on a PerkinElmer Spectrum One FT-IR spectrometer equipped with a universal ATR sampling accessory. Thermogravimetric analysis was performed on a PerkinElmer Pyrus 1 TGA instrument equipped with an ultramicro balance with a sensitivity of 0.1 μg. The temperature range was from 25 to 500 °C with a scan rate of 5 °C/min (Figures S6 and S7). Emission (fluorescence, phosphorescence, and excitation) spectra and lifetimes were recorded on a Varian Cary Eclipse Fluorimeter at 298 K. Phosphorescence data were collected between 570 and 720 nm for Eu(III) emission and between 565 and 575 nm for Tb(III) emission with a measurement delay time of 0.1 ms. Phosphorescence lifetimes of the Ln(III) excited states were measured in the time-resolved mode at 298 K. Elemental analysis was carried out on an Exeter Analytical CE440 elemental analyzer at the microanalysis laboratory at the School of Chemistry and Chemical Biology, University College Dublin. Phase purity of all crystalline materials was confirmed with X-ray powder diffraction patterns recorded with a Bruker D2 Phaser instrument using Cu Kα (λ = 1.5405 Å) radiation. Samples were finely ground and applied to a quartz sample holder. Data were measured at room temperature in the 2θ range of 5−55° in 0.01° increments with concurrent rotation in φ of 1 rpm. Additional X-ray powder diffraction data for **1** were collected at 100 K on a Bruker Apex-II Duo instrument using Cu Kα radiation in the 2θ range of 2−55° and converted to θ vs intensity data by integration of Debye rings obtained from the area detector data. Raw data were compared with the simulated patterns from the single crystal data collections carried out at 100 K (Figures S28, S29, and S33). Gas adsorption isotherms were measured using a Quantachrome Autosorb IQ gas sorption analyzer. Chemically pure (CP, N4.5) grade He, N_2, H_2, and CO_2 gases were used for the measurements.

Crystallography. Single crystal X-ray data for $\mathbf{H_3L}$ were collected at 100 K on a Rigaku AFC12 goniometer equipped with an enhanced sensitivity (HG) Saturn 724+ detector mounted at the window of an FR-E+ Superbright Mo Kα rotating anode generator (λ = 0.71075 Å) with HF varimax optics.[35] Unit cell parameters were refined against all data and an empirical absorption correction applied in CrystalClear.[36] The data for $\mathbf{H_3L}$ were solved by direct methods using SHELXS-2013[37] and refined on F_0^2 by SHELXL-2013[37] using ShelXle.[38] Hydrogen atoms (except OH protons which were found from the difference map and then fixed with $U_{iso} = 1.2U_{eq}(O)$) were positioned geometrically and refined using a riding model with d(CH) = 0.95 Å, $U_{iso} = 1.2U_{eq}$(C) for aromatic protons, d(CH) = 0.99 Å, $U_{iso} = 1.2U_{eq}$(C) for CH_2. All non-hydrogen atoms were refined anisotropically.

X-ray data for **1** and **2** were collected on a Bruker APEX-II DUO diffractometer using microfocus Cu Kα (λ = 1.5405 Å) radiation. All data collections were carried out using standard ω and φ scans at 100 K with temperature control provided by a Cobra cryostream. The data were reduced and multiscan absorption corrections applied using SADABS[39] within the Bruker APEX3 software suite.[40] All data sets were solved with direct methods using SHELXS[37] and refined on F^2 by full-matrix least-squares procedures with SHELXL-2014[41] within the OLEX-2 GUI.[42] All non-hydrogen atoms were freely refined with anisotropic displacement parameters, while hydrogen atoms were assigned to geometric positions and refined with a riding model with U_{iso} equivalent to 1.2 or 1.5 times the isotropic equivalent of the carrier atom. The data sets for **1** and **2** contained regions of diffuse electron density consistent with delocalized lattice solvent molecules. The diffuse electron density regions' scattering contribution to the measured structure factors was accounted for using SQUEEZE allowing for more representative refinement statistics for the framework atoms.[31] The solvent channel contents were ascertained using TGA, NMR, and elemental analysis, and a discussion of the correlation of each with the SQUEEZE calculations can be found in the Supporting Information.

Synthetic Procedures. *Synthesis of H_3L.* Synthesis of $\mathbf{H_3L}$ was carried out according to a literature procedure.[12c]

*Synthesis of Poly-[Zn_7L_6]·(H_2NMe_2)$_4$·(H_2O)$_{45}$ (**1**).* To a 95:5 DMF/H_2O mixture (1 mL) were added $\mathbf{H_3L}$ (15 mg, 0.029 mmol, 1 equiv) and zinc(II) nitrate hexahydrate (11 mg, 0.036 mmol, 1.2 equiv), and the mixture was sealed and heated at 100 °C for 40 h. The resulting faint yellow crystals were isolated by filtration, washed with DMF, and dried under suction: 13 mg, 0.021 mmol, 72%; mp 348−351 °C dec; found C 42.73, H 4.10, N 14.49, calculated for −[Zn_7L_6]·(H_2NMe_2)$_4$·(H_2O)$_{45}$, i.e., $C_{164}H_{218}N_{46}O_{81}Zn_7$, C 42.97, H 4.78, N 14.06; IR υ_{max} (cm^{-1}) 2977 br, 2371, 2296, 2253, 2044, 1610, 1560, 1550, 1442, 1357, 1258, 1180, 1066, 1019, 907, 861, 851, 839, 817, 791, 773, 761, 738, 728, 717, 705, 694, 684, 672, 659. Phase purity was supported by X-ray powder diffraction (Figure S29).

*Synthesis of Poly-[Zn**HL**] (**2**).* Compound **2** formed as a side-product impurity in the synthesis of **1**. It was characterized by single crystal and powder X-ray diffraction analysis. There were difficulties in optimizing the synthetic conditions required to produce pure phase **2**. Ensuring there was a slight excess of zinc(II) nitrate hexahydrate (1.2 equiv with respect to $\mathbf{H_3L}$) gave rise to pure phase **1**.

ASSOCIATED CONTENT

Supporting Information

The Supporting Information is available free of charge on the ACS Publications website at DOI: 10.1021/acs.inorgchem.8b00080.

Crystallography, thermogravimetric analysis, gas adsorption studies, IR data, modeled solvent channel occupancies, NMR data, cation exchange experiments, Ln(III) sensitization studies, and powder XRD and structural studies of second crystallographic phase poly-[Zn(**HL**)] (**2**) (PDF)

Accession Codes

CCDC 1582309−1582311 contain the supplementary crystallographic data for this paper. These data can be obtained free of charge via www.ccdc.cam.ac.uk/data_request/cif, or by emailing data_request@ccdc.cam.ac.uk, or by contacting The Cambridge Crystallographic Data Centre, 12 Union Road, Cambridge CB2 1EZ, UK; fax: +44 1223 336033.

AUTHOR INFORMATION

Corresponding Author

*E-mail: gunnlaut@tcd.ie.

ORCID

Eoin P. McCarney: 0000-0001-7693-6719
Chris S. Hawes: 0000-0001-6902-7939
Jonathan A. Kitchen: 0000-0002-7139-5666
Thorfinnur Gunnlaugsson: 0000-0003-4814-6853

Present Address

[‖]Institute of Natural and Mathematical Sciences, Massey University Albany, Auckland 0745, New Zealand

Author Contributions

The manuscript was written through contributions of all authors. All authors have given approval to the final version of the manuscript.

DOI: 10.1021/acs.inorgchem.8b00080
Inorg. Chem. XXXX, XXX, XXX−XXX

Funding

We would like to thank the Irish Research Council (IRC) for both a postgraduate scholarship (to E.P.M.) (GOIPG/2013/452) and a postdoctoral fellowship (to C.S.H.) (GOIPD/2015/446), Science Foundation Ireland (SFI) (PI Awards 10/45 IN.1/B2999 and 13/IA/1865 to T.G.), and the European Research Council (ERC; CoG 2014−647719 to W.S.) for financial support. We would like to specially thank Dr. Brendan Twamley for his dedication and training (E.P.M.) in the use of X-ray crystallography.

Notes

The authors declare no competing financial interest.

REFERENCES

(1) (a) O'Keeffe, M.; Yaghi, O. M. Deconstructing the Crystal Structures of Metal−Organic Frameworks and Related Materials into Their Underlying Nets. *Chem. Rev.* **2012**, *112*, 675−702. (b) Cui, X.; Chen, K.-J.; Xing, H.; Yang, Q.; Krishna, R.; Bao, Z.; Wu, H.; Zhou, W.; Dong, X.; Han, Y.; Li, B.; Ren, Q.; Zaworotko, M. J.; Chen, B. Pore chemistry and size control in hybrid porous materials for acetylene capture from ethylene. *Science* **2016**, *353*, 141−144. (c) Li, M.; Li, D.; O'Keeffe, M.; Yaghi, O. M. Topological Analysis of Metal-Organic Frameworks with Polytopic Linkers and/or Multiple Building Units and the Minimal Transitivity Principle. *Chem. Rev.* **2014**, *114*, 1343−1370.

(2) (a) Furukawa, H.; Cordova, K. E.; O'Keeffe, M.; Yaghi, O. M. The Chemistry and Applications of Metal-Organic Frameworks. *Science* **2013**, *341*, 1230444. (b) Zhang, Z.; Zaworotko, M. J. Template-directed synthesis of metal-organic materials. *Chem. Soc. Rev.* **2014**, *43*, 5444−5455. (c) O'Nolan, D.; Kumar, A.; Zaworotko, M. J. *J. Am. Chem. Soc.* **2017**, *139*, 8508−8513.

(3) (a) Lee, J. Y.; Farha, O. K.; Roberts, J.; Scheidt, K. A.; Nguyen, S. B. T.; Hupp, J. T. Metal-organic framework materials as catalysts. *Chem. Soc. Rev.* **2009**, *38*, 1450−1459. (b) Moon, H. R.; Lim, D.-W.; Suh, M. P. Fabrication of metal nanoparticles in metal-organic frameworks. *Chem. Soc. Rev.* **2013**, *42*, 1807−1824. (c) Gao, X.; Liu, M.; Lan, J.; Liang, L.; Zhang, X.; Sun, J. Lewis Acid-Base Bifunctional Crystals with a Three-Dimensional Framework for Selective Coupling of CO2 and Epoxides under Mild and Solvent-Free Conditions. *Cryst. Growth Des.* **2017**, *17*, 51−57.

(4) (a) Dunning, S. G.; Nuñez, A. J.; Moore, M. D.; Steiner, A.; Lynch, V. M.; Sessler, J. L.; Holliday, B. J.; Humphrey, S. M. A Sensor for Trace H_2O Detection in D_2O. *Chem.* **2017**, *2*, 579−589. (b) Wang, J.; Sun, W.; Chang, S.; Liu, H.; Zhang, G.; Wang, Y.; Liu, Z. A terbium metal-organic framework with stable luminescent emission in a wide pH range that acts as a quantitative detection material for nitroaromatics. *RSC Adv.* **2015**, *5*, 48574−48579. (c) Wang, Y.-Q.; Tan, Q.-H.; Liu, H.-T.; Sun, W.; Liu, Z.-L. A luminescent europium MOF containing Lewis basic pyridyl site for highly selective sensing of o-, m- and p-nitrophenol. *RSC Adv.* **2015**, *5*, 86614−86619. (d) Kreno, L. E.; Leong, K.; Farha, O. K.; Allendorf, M.; Van Duyne, R. P.; Hupp, J. T. Metal-Organic Framework Materials as Chemical Sensors. *Chem. Rev.* **2012**, *112*, 1105−1125.

(5) Chen, C.-X.; Liu, Q.-K.; Ma, J.-P.; Dong, Y.-B. Encapsulation of Ln3+ hydrate species for tunable luminescent materials based on a porous Cd(ii)-MOF. *J. Mater. Chem.* **2012**, *22*, 9027−9033.

(6) (a) Chaemchuen, S.; Kabir, N. A.; Zhou, K.; Verpoort, F. Metal-organic frameworks for upgrading biogas via CO2 adsorption to biogas green energy. *Chem. Soc. Rev.* **2013**, *42*, 9304−9332. (b) Eddaoudi, M.; Kim, J.; Rosi, N.; Vodak, D.; Wachter, J.; O'Keeffe, M.; Yaghi, O. M. Systematic design of pore size and functionality in isoreticular MOFs and their application in methane storage. *Science* **2002**, *295*, 469−472. (c) Moellmer, J.; Lange, M.; Moeller, A.; Patzschke, C.; Stein, K.; Laessig, D.; Lincke, J.; Glaeser, R.; Krautscheid, H.; Staudt, R. Pure and mixed gas adsorption of CH4 and N2 on the metal-organic framework Basolite A100 and a novel copper-based 1,2,4-triazolyl isophthalate MOF. *J. Mater. Chem.* **2012**, *22*, 10274−10286. (d) Thallapally, P. K.; Tian, J.; Radha Kishan, M.; Fernandez, C. A.; Dalgarno, S. J.; McGrail, P. B.; Warren, J. E.; Atwood, J. L. Flexible (Breathing) Interpenetrated Metal-Organic Frameworks for CO2 Separation Applications. *J. Am. Chem. Soc.* **2008**, *130*, 16842−16843. (e) Reichenbach, C.; Kalies, G.; Lincke, J.; Lässig, D.; Krautscheid, H.; Moellmer, J.; Thommes, M. Unusual adsorption behavior of a highly flexible copper-based MOF. *Microporous Mesoporous Mater.* **2011**, *142*, 592−600. (f) Lincke, J.; Lässig, D.; Kobalz, M.; Bergmann, J.; Handke, M.; Möllmer, J.; Lange, M.; Roth, C.; Möller, A.; Staudt, R.; Krautscheid, H. An Isomorphous Series of Cubic, Copper-Based Triazolyl Isophthalate MOFs: Linker Substitution and Adsorption Properties. *Inorg. Chem.* **2012**, *51*, 7579−7586.

(7) (a) Lin, Z.-J.; Lu, J.; Hong, M.; Cao, R. Metal-organic frameworks based on flexible ligands (FL-MOFs): structures and applications. *Chem. Soc. Rev.* **2014**, *43*, 5867−5895. (b) Liu, T.-F.; Lu, J.; Tian, C.; Cao, M.; Lin, Z.; Cao, R. Porous Anionic, Cationic, and Neutral Metal-Carboxylate Frameworks Constructed from Flexible Tetrapodal Ligands: Syntheses, Structures, Ion-Exchanges, and Magnetic Properties. *Inorg. Chem.* **2011**, *50*, 2264−2271. (c) Hong, M.; Zhao, Y.; Su, W.; Cao, R.; Fujita, M.; Zhou, Z.; Chan, A. S. C. A silver(I) coordination polymer chain containing nanosized tubes with anionic and solvent molecule guests. *Angew. Chem., Int. Ed.* **2000**, *39*, 2468−2470. (d) Xu, B.; Lin, X.; He, Z.; Lin, Z.; Cao, R. A unique 2D 3D polycatenation cobalt(II)-based molecule magnet showing coexistence of paramagnetism and canted antiferromagnetism. *Chem. Commun.* **2011**, *47*, 3766−3768.

(8) (a) Schneemann, A.; Bon, V.; Schwedler, I.; Senkovska, I.; Kaskel, S.; Fischer, R. A. Flexible metal-organic frameworks. *Chem. Soc. Rev.* **2014**, *43*, 6062−6096. (b) Hawes, C. S.; Byrne, K.; Schmitt, W.; Gunnlaugsson, T. Flexible Porous Coordination Polymers from Divergent Photoluminescent 4-Oxo-1,8-naphthalimide Ligands. *Inorg. Chem.* **2016**, *55*, 11570−11582. (c) Hawes, C. S.; Knowles, G. P.; Chaffee, A. L.; Turner, D. R.; Batten, S. R. Modulating Porosity through Conformer-Dependent Hydrogen Bonding in Copper(II) Coordination Polymers. *Cryst. Growth Des.* **2015**, *15*, 3417−3425.

(9) Batten, S. R. N.; Neville, S. M.; Turner, D. R. *Coordination Polymers: Design, Analysis and Application*; RSC Publishing: Cambridge, U.K., 2009.

(10) (a) James, S. L. Metal-organic frameworks. *Chem. Soc. Rev.* **2003**, *32*, 276−288. (b) Ma, M.-L.; Qin, J.-H.; Ji, C.; Xu, H.; Wang, R.; Li, B.-J.; Zang, S.-Q.; Hou, H.-W.; Batten, S. R. Anionic porous metal-organic framework with novel 5-connected vbk topology for rapid adsorption of dyes and tunable white light emission. *J. Mater. Chem. C* **2014**, *2*, 1085−1093. (c) Ma, Y.; Li, X.; Li, A.; Yang, P.; Zhang, C.; Tang, B. H_2S-Activable MOF Nanoparticle Photosensitizer for Effective Photodynamic Therapy against Cancer with Controllable Singlet-Oxygen Release. *Angew. Chem., Int. Ed.* **2017**, *56*, 13752−13756. (d) Kang, X.-M.; Cheng, R.-R.; Xu, H.; Wang, W.-M.; Zhao, B. A Sensitive Luminescent Probe of Acetylacetone based on ZnMOF with Six-Fold Interpenetration. *Chem. - Eur. J.* **2017**, *23*, 13289. (e) Hou, S.-L.; Dong, J.; Jiang, X.-L.; Jiao, Z.-H.; Wang, C.-M.; Zhao, B. Interpenetration-Depended Luminescent Probe in IndiumOrganic Frameworks for Selectively Detecting Nitrofurazone in Water. *Anal. Chem.* **2018**, *90*, 1516. (f) Xu, H.; Zhai, B.; Cao, C.-S.; Zhao, B. A Bifunctional Europium−Organic Framework with Chemical Fixation of CO_2 and Luminescent Detection of Al^{3+}. *Inorg. Chem.* **2016**, *55*, 9671.

(11) (a) Johnson, J. A.; Finn, M. G.; Koberstein, J. T.; Turro, N. J. Construction of linear polymers, dendrimers, networks, and other polymeric architectures by copper-catalyzed azide-alkyne cycloaddition "click" chemistry. *Macromol. Rapid Commun.* **2008**, *29*, 1052−1072. (b) Zhang, C.; Shen, X.; Sakai, R.; Gottschaldt, M.; Schubert, U. S.; Hirohara, S.; Tanihara, M.; Yano, S.; Obata, M.; Xiao, N.; Satoh, T.; Kakuchi, T. Syntheses of 3-arm and 4-arm star-branched polystyrene Ru(II) complexes by the click-to-chelate approach. *J. Polym. Sci., Part A: Polym. Chem.* **2011**, *49*, 746−753. (c) Munuera, L.; O'Reilly, R. K. Using metal-ligand interactions for the synthesis of metallostar polymers. *Dalton Trans.* **2010**, *39*, 388−391. (d) Xiao, N.; Chen, Y.; Shen, X.; Zhang, C.; Yano, S.; Gottschaldt, M.; Schubert, U. S.;

DOI: 10.1021/acs.inorgchem.8b00080
Inorg. Chem. XXXX, XXX, XXX−XXX

Kakuchi, T.; Satoh, T. Synthesis of miktoarm star copolymer Ru(II) complexes by click-to-chelate approach. *Polym. J.* **2013**, *45*, 216−225. (e) Byrne, J. P.; Kitchen, J. A.; Gunnlaugsson, T. The btp [2,6-bis(1,2,3-triazol-4-yl)pyridine] binding motif: a new versatile terdentate ligand for supramolecular and coordination chemistry. *Chem. Soc. Rev.* **2014**, *43*, 5302−5325.

(12) (a) Meudtner, R. M.; Hecht, S. Responsive backbones based on alternating triazole-pyridine/benzene copolymers: from helically folding polymers to metallosupramolecularly crosslinked gels. *Macromol. Rapid Commun.* **2008**, *29*, 347−351. (b) Meudtner, R. M.; Hecht, S. Helicity inversion in responsive foldamers induced by achiral halide ion guests. *Angew. Chem., Int. Ed.* **2008**, *47*, 4926−4930. (c) McCarney, E. P.; Byrne, J. P.; Twamley, B.; Martinez-Calvo, M.; Ryan, G.; Mobius, M. E.; Gunnlaugsson, T. Self-assembly formation of a healable lanthanide luminescent supramolecular metallogel from 2,6-bis(1,2,3-triazol-4-yl)pyridine (btp) ligands. *Chem. Commun.* **2015**, *51*, 14123−14126. (d) Byrne, J. P.; Kitchen, J. A.; Kotova, O.; Leigh, V.; Bell, A. P.; Boland, J. J.; Albrecht, M.; Gunnlaugsson, T. Synthesis, structural, photophysical and electrochemical studies of various d-metal complexes of btp [2,6-bis(1,2,3-triazol-4-yl)pyridine] ligands that give rise to the formation of metallo-supramolecular gels. *Dalton Trans.* **2014**, *43*, 196−209.

(13) (a) Zou, J.-Y.; Gao, H.-L.; Shi, W.; Cui, J.-Z.; Cheng, P. Auxiliary ligand-assisted structural diversities of three metal-organic frameworks with potassium 1H-1,2,3-triazole-4,5-dicarboxylic acid. Syntheses, crystal structures and luminescence properties. *CrystEngComm* **2013**, *15*, 2682−2687. (b) Seth, S.; Savitha, G.; Moorthy, J. N. Carbon Dioxide Capture by a Metal−Organic Framework with Nitrogen-Rich Channels Based on Rationally Designed Triazole-Functionalized Tetraacid Organic Linker. *Inorg. Chem.* **2015**, *54*, 6829−6835. (c) Zhang, Z.; Xiang, S.; Chen, Y.-S.; Ma, S.; Lee, Y.; Phely-Bobin, T.; Chen, B. A Robust Highly Interpenetrated Metal-Organic Framework Constructed from Pentanuclear Clusters for Selective Sorption of Gas Molecules. *Inorg. Chem.* **2010**, *49*, 8444−8448. (d) Devic, T.; David, O.; Valls, M.; Marrot, J.; Couty, F.; Ferey, G. An Illustration of the Limit of the Metal Organic Framework's Isoreticular Principle Using a Semirigid Tritopic Linker Obtained by "Click" Chemistry. *J. Am. Chem. Soc.* **2007**, *129*, 12614−12615. (e) Yan, Y.; Suyetin, M.; Bichoutskaia, E.; Blake, A. J.; Allan, D. R.; Barnett, S. A.; Schroeder, M. Modulating the packing of [Cu24(isophthalate)24] cuboctahedra in a triazole-containing metal-organic polyhedral framework. *Chem. Sci.* **2013**, *4*, 1731−1736. (f) Wang, X.-J.; Li, P.-Z.; Chen, Y.; Zhang, Q.; Zhang, H.; Chan, X. X.; Ganguly, R.; Li, Y.; Jiang, J.; Zhao, Y. A rationally designed nitrogen-rich metal-organic framework and its exceptionally high CO2 and H2 uptake capability. *Sci. Rep.* **2013**, *3* (1149), 5.

(14) (a) Khatua, S.; Kumar Bar, A.; Konar, S. Tuning Proton Conductivity by Interstitial Guest Change in Size-Adjustable Nanopores of a CuI-MOF: A Potential Platform for Versatile Proton Carriers. *Chem. - Eur. J.* **2016**, *22*, 16277−16285. (b) Handke, M.; Weber, H.; Lange, M.; Möllmer, J.; Lincke, J.; Gläser, R.; Staudt, R.; Krautscheid, H. Network Flexibility: Control of Gate Opening in an Isostructural Series of Ag-MOFs by Linker Substitution. *Inorg. Chem.* **2014**, *53*, 7599−7607. (c) Hernandez-Gil, J.; Ferrer, S.; Castineiras, A.; Lloret, F. A unique discrete tetranuclear Cu'-Cu(N-N)2Cu-Cu' copper(II) complex, built from a μ3−1,2,4-triazolato-μ-carboxylato ligand, as an effective DNA cleavage agent. *Inorg. Chem.* **2012**, *51*, 9809−19. (d) Naik, A. D.; Dirtu, M. M.; Railliet, A. P.; Marchand-Brynaert, J.; Garcia, Y. Coordination Polymers and Metal Organic Frameworks Derived from 1,2,4-Triazole Amino Acid Linkers. *Polymers* **2011**, *3*, 1750. (e) Kobalz, M.; Lincke, J.; Kobalz, K.; Erhart, O.; Bergmann, J.; Laessig, D.; Lange, M.; Moellmer, J.; Glaeser, R.; Staudt, R.; Krautscheid, H. Paddle Wheel Based Triazolyl Isophthalate MOFs: Impact of Linker Modification on Crystal Structure and Gas Sorption Properties. *Inorg. Chem.* **2016**, *55*, 3030−3039. (f) Li, J.-R.; Sculley, J.; Zhou, H.-C. Metal-Organic Frameworks for Separations. *Chem. Rev.* **2012**, *112*, 869−932.

(15) (a) Li, Y.; Huffman, J. C.; Flood, A. H. Can terdentate 2,6-bis(1,2,3-triazol-4-yl)pyridines form stable coordination compounds? *Chem. Commun.* **2007**, 2692−2694. (b) Ostermeier, M.; Berlin, M.-A.; Meudtner, R. M.; Demeshko, S.; Meyer, F.; Limberg, C.; Hecht, S. Complexes of Click-Derived Bistriazolylpyridines: Remarkable Electronic Influence of Remote Substituents on Thermodynamic Stability as well as Electronic and Magnetic Properties. *Chem. - Eur. J.* **2010**, *16*, 10202−10213.

(16) Chandrasekhar, N.; Chandrasekar, R. "Click-Fluors": Synthesis of a Family of π-Conjugated Fluorescent Back-to-Back Coupled 2,6-Bis(triazol-1-yl)pyridines and Their Self-Assembly Studies. *J. Org. Chem.* **2010**, *75*, 4852−4855.

(17) (a) Crowley, J. D.; Bandeen, P. H. A multicomponent CuAAC "click" approach to a library of hybrid polydentate 2-pyridyl-1,2,3-triazole ligands: new building blocks for the generation of metallosupramolecular architectures. *Dalton Trans.* **2010**, *39*, 612−623. (b) Meudtner, R. M.; Ostermeier, M.; Goddard, R.; Limberg, C.; Hecht, S. Multifunctional "Clickates" as Versatile Extended Heteroaromatic Building Blocks: Efficient Synthesis via Click Chemistry, Conformational Preferences, and Metal Coordination. *Chem. - Eur. J.* **2007**, *13*, 9834−9840. (c) Fletcher, J. T.; Walz, S. E.; Keeney, M. E. Monosubstituted 1,2,3-triazoles from two-step one-pot deprotection/click additions of trimethylsilylacetylene. *Tetrahedron Lett.* **2008**, *49*, 7030−7032.

(18) Kobalz, K.; Kobalz, M.; Möllmer, J.; Junghans, U.; Lange, M.; Bergmann, J.; Dietrich, S.; Wecks, M.; Gläser, R.; Krautscheid, H. Bis(carboxyphenyl)-1,2,4-triazole Based Metal−Organic Frameworks: Impact of Metal Ion Substitution on Adsorption Performance. *Inorg. Chem.* **2016**, *55*, 6938−6948.

(19) (a) Crowley, J. D.; Bandeen, P. H.; Hanton, L. R. A one pot multi-component CuAAC "click" approach to bidentate and tridentate pyridyl-1,2,3-triazole ligands: Synthesis, X-ray structures and copper(II) and silver(I) complexes. *Polyhedron* **2010**, *29*, 70−83. (b) Byrne, J. P.; Blasco, S.; Aletti, A. B.; Hessman, G.; Gunnlaugsson, T. Formation of Self-Templated 2,6-Bis(1,2,3-triazol-4-yl)pyridine [2]Catenanes by Triazolyl Hydrogen Bonding: Selective Anion Hosts for Phosphate. *Angew. Chem., Int. Ed.* **2016**, *55*, 8938−8943. (c) Byrne, J. P.; Martínez-Calvo, M.; Peacock, R. D.; Gunnlaugsson, T. Chiroptical Probing of Lanthanide-Directed Self-Assembly Formation Using btp Ligands Formed in One-Pot Diazo-Transfer/Deprotection Click Reaction from Chiral Amines. *Chem. - Eur. J.* **2016**, *22*, 486−490. (d) Fitchett, C. M.; Richardson, C.; Steel, P. J. Solid state conformations of symmetrical aromatic biheterocycles: an X-ray crystallographic investigation. *Org. Biomol. Chem.* **2005**, *3*, 498−502. (e) Schweinfurth, D.; Hardcastle, K. I.; Bunz, U. H. F. 1,3-Dipolar cycloaddition of alkynes to azides. Construction of operationally functional metal responsive fluorophores. *Chem. Commun.* **2008**, 2203−2205. (f) McMorran, D. A. Ag(I)-Based Tectons for the Construction of Helical and meso-Helical Hydrogen-Bonded Coordination Networks. *Inorg. Chem.* **2008**, *47*, 592−601. (g) McCarney, E. P.; Hawes, C. S.; Blasco, S.; Gunnlaugsson, T. Synthesis and structural studies of 1,4-di(2-pyridyl)-1,2,3-triazole dpt and its transition metal complexes; a versatile and subtly unsymmetric ligand. *Dalton Trans.* **2016**, *45*, 10209−10221.

(20) (a) Tobin, G.; Comby, S.; Zhu, N.; Clerac, R.; Gunnlaugsson, T.; Schmitt, W. Towards multifunctional lanthanide-based metal−organic frameworks. *Chem. Commun.* **2015**, *51*, 13313−13316. (b) Xiao, Y.; Wang, S.-H.; Zheng, F.-K.; Wu, M.-F.; Xu, J.; Liu, Z.-F.; Chen, J.; Li, R.; Guo, G.-C. Excitation wavelength-induced color-tunable and white-light emissions in lanthanide(iii) coordination polymers constructed using an environment-dependent luminescent tetrazolate-dicarboxylate ligand. *CrystEngComm* **2016**, *18*, 721−727. (c) Huang, W.; Pan, F.; Liu, Y.; Huang, S.; Li, Y.; Yong, J.; Li, Y.; Kirillov, A. M.; Wu, D. An Efficient Blue-Emissive Metal−Organic Framework (MOF) for Lanthanide-Encapsulated Multicolor and Stimuli-Responsive Luminescence. *Inorg. Chem.* **2017**, *56*, 6362−6370.

(21) Karmakar, A.; Samanta, P.; Desai, A. V.; Ghosh, S. K. Guest-Responsive Metal−Organic Frameworks as Scaffolds for Separation and Sensing Applications. *Acc. Chem. Res.* **2017**, *50*, 2457.

(22) Fritzsche, J. C.; Grzywa, M.; Denysenko, D.; Bon, V.; Senkovska, I.; Kaskel, S.; Volkmer, D. CFA-4 - a fluorinated metal-

DOI: 10.1021/acs.inorgchem.8b00080
Inorg. Chem. XXXX, XXX, XXX−XXX

organic framework with exchangeable interchannel cations. *Dalton Trans.* **2017**, *46*, 6745−6755.
(23) (a) Cui, Y.; Yue, Y.; Qian, G.; Chen, B. Luminescent Functional Metal−Organic Frameworks. *Chem. Rev.* **2012**, *112*, 1126−1162. (b) Wu, H.; Ying, L.; Yang, W.; Cao, Y. Progress and perspective of polymer white light-emitting devices and materials. *Chem. Soc. Rev.* **2009**, *38*, 3391−3400.
(24) Ma, M.-L.; Qin, J.-H.; Ji, C.; Xu, H.; Wang, R.; Li, B.-J.; Zang, S.-Q.; Hou, H.-W.; Batten, S. R. Batten, S. R., Anionic porous metal-organic framework with novel 5-connected vbk topology for rapid adsorption of dyes and tunable white light emission. *J. Mater. Chem. C* **2014**, *2*, 1085−1093.
(25) (a) *The GAVROG Project, Systre 1.2.0*; 2004; http://gavrog.org/. (b) Delgado-Friedrichs, O.; O'Keeffe, M. Identification of and symmetry computation for crystal nets. *Acta Crystallogr., Sect. A: Found. Crystallogr.* **2003**, *59*, 351−360.
(26) Etter, M. C. Encoding and decoding hydrogen-bond patterns of organic compounds. *Acc. Chem. Res.* **1990**, *23*, 120−6.
(27) (a) Kilpin, K. J.; Crowley, J. D. Palladium(II) and platinum(II) complexes of bidentate 2-pyridyl-1,2,3-triazole "click" ligands: Synthesis, properties and X-ray structures. *Polyhedron* **2010**, *29*, 3111−3117. (b) Danielraj, P.; Varghese, B.; Sankararaman, S. 2,6-Bis(1-benzyl-1H-1,2,3-triazol-4-yl)pyridine and its octahedral copper complex. *Acta Crystallogr., Sect. C: Cryst. Struct. Commun.* **2010**, *66*, m366−m370. (c) Midya, G. C.; Paladhi, S.; Bhowmik, S.; Saha, S.; Dash, J. Design and synthesis of an on-off "click" fluorophore that executes a logic operation and detects heavy and transition metal ions in water and living cells. *Org. Biomol. Chem.* **2013**, *11*, 3057−3063.
(28) (a) Estroff, L. A.; Hamilton, A. D. Water Gelation by Small Organic Molecules. *Chem. Rev.* **2004**, *104*, 1201−1218. (b) Piepenbrock, M.-O. M.; Lloyd, G. O.; Clarke, N.; Steed, J. W. Metal- and Anion-Binding Supramolecular Gels. *Chem. Rev.* **2010**, *110*, 1960−2004. (c) Yang, L.; Tan, X.; Wang, Z.; Zhang, X. Supramolecular Polymers: Historical Development, Preparation, Characterization, and Functions. *Chem. Rev.* **2015**, *115*, 7196−7239.
(29) Pavia, D. L.; Lampman, G. M.; Kriz, G. S. *Introduction to Spectroscopy*, 3rd ed.; Thomson: Bellingham, WA, 2001.
(30) Burrows, A. D.; Cassar, K.; Friend, R. M. W.; Mahon, M. F.; Rigby, S. P.; Warren, J. E. Solvent hydrolysis and templating effects in the synthesis of metal-organic frameworks. *CrystEngComm* **2005**, *7*, 548−550.
(31) Spek, A. L. PLATON SQUEEZE. *Acta Crystallogr., Sect. C: Struct. Chem.* **2015**, *71*, 9−18.
(32) Yang, L.; Powell, D. R.; Houser, R. P. Structural variation in copper(i) complexes with pyridylmethylamide ligands: structural analysis with a new four-coordinate geometry index, [small tau]4. *Dalton Trans.* **2007**, 955−964.
(33) (a) Delgado Friedrichs, O.; O'Keeffe, M.; Yaghi, O. M. Three-periodic nets and tilings: semiregular nets. *Acta Crystallogr., Sect. A: Found. Crystallogr.* **2003**, *59*, 515−525. (b) O'Keeffe, M.; Peskov, M. A.; Ramsden, S. J.; Yaghi, O. M. The Reticular Chemistry Structure Resource (RCSR) database of, and symbols for, crystal nets. *Acc. Chem. Res.* **2008**, *41*, 1782−1789.
(34) Byrne, J. P.; Kitchen, J. A.; O'Brien, J. E.; Peacock, R. D.; Gunnlaugsson, T. Lanthanide Directed Self-Assembly of Highly Luminescent Supramolecular "Peptide" Bundles from α-Amino Acid Functionalized 2,6-Bis(1,2,3-triazol-4-yl)pyridine (btp) Ligands. *Inorg. Chem.* **2015**, *54*, 1426−1439.
(35) Coles, S. J.; Gale, P. A. Changing and challenging times for service crystallography. *Chemical Science* **2012**, *3*, 683−689.
(36) *CrystalClear-SM Expert 3.1*; Rigaku: 2012.
(37) Sheldrick, G. M. A short history of SHELX. *Acta Crystallogr., Sect. A: Found. Crystallogr.* **2008**, *64*, 112−122.
(38) Huebschle, C. B.; Sheldrick, G. M.; Dittrich, B. ShelXle: a Qt graphical user interface for SHELXL. *J. Appl. Crystallogr.* **2011**, *44*, 1281−1284.
(39) *SADABS*; Bruker-AXS Inc.: Madison, WI, 2001.
(40) *Bruker APEX3*; Bruker-AXS Inc.: Madison, WI, 2015.
(41) Sheldrick, G. M. Crystal structure refinement with SHELXL. *Acta Crystallogr., Sect. C: Struct. Chem.* **2015**, *71*, 3−8.
(42) Dolomanov, O. V.; Bourhis, L. J.; Gildea, R. J.; Howard, J. A. K.; Puschmann, H. OLEX2: a complete structure solution, refinement and analysis program. *J. Appl. Crystallogr.* **2009**, *42*, 339−341.

DOI: 10.1021/acs.inorgchem.8b00080
Inorg. Chem. XXXX, XXX, XXX−XXX